ANALYSIS OF THE IMPACT OF THE INLET BOUNDARY CONDITIONS IN FDS RESULTS FOR AIR CURTAIN FLOWS IN THE NEAR-FIELD REGION

L.-X. Yu[1, 2], F. Liu[1], B. Merci[2]

Fangliu@cqu.edu.cn (F. Liu)

[1]Chongqing University, Faculty of Urban Construction and Environmental Engineering

[2]Ghent University – UGent, Dept. of Flow, Heat and Combustion Mechanics

Abstract:

CFD results are discussed for planar jet flows, resembling configurations in use for air curtain flows in the context of smoke and heat control in buildings in case of fire. The CFD package FDS (Fire Dynamics Simulator), Version 6.0.1, is used. Special focus is given to the impact of the inlet boundary condition, in combination with the mesh size, on the flow field in the near-field region. Investigation of different slot configurations, including calculations inside a straight rectangular duct ahead of the air slot, reveals a small vena contracta effect when the slot is flush with a solid boundary, leading to an acceleration of the flow in the symmetry plane in the near-field region. More important is the effect of the duct length: starting from a top hat velocity profile, a duct length of about 15 hydraulic diameters is required for the flow to become fully developed at the slot. The vena contracta effect disappears if the co-flow at the nozzle exit is aligned with the jet. The FDS results capture the self-similarity in the far-field jet region, regardless of the inlet configuration.

Key words: CFD; FDS; Velocity Inlet Boundary condition; Air curtain; Planar Jet flows

1. Introduction

Smoke has been reported to be the most fatal factor in fires. In order to prevent the smoke from causing a harmful environment for the building occupants, a smoke and heat control system can be applied to control and remove heat and smoke induced by fire. For instance, the pressurization of stairwells is a commonly used smoke control system in buildings. However, large air supply volumes are required. Therefore, an air curtain could be a more efficient way of blocking smoke dispersion during fires[1].

Air curtains can be considered as compartmentation devices, based on the discharge of a plane jet. Therefore, it is interesting to study plane jets, particularly in the so-called 'near-field region', i.e., the region close to the air slot. Indeed, air curtains operate in regions not far from the nozzle exits. It is worth noting that plane jets have also found their practical application in a variety of industrial applications. Some of the major applications of jets occur in preventing leakage of flammable gases from reaching industrial furnaces[2, 3], in reducing dispersed pollution in urban road tunnels[4], in controlling pollutant spreading for emergency management in cleanrooms[5], or in preserving low temperatures in the refrigerated storage rooms[6] and food display cabinets[7].

In the context of fire, air curtains can be used to prevent smoke spreading from one volume to an adjacent volume. According to People's Republic of China Machinery Industry Standard: Air Curtain (JB/T 9067－1999), the nominal velocity of outlet is 4-9m/s for commercial and civil building, and 8-24m/s for industrial building[8]. In recent years, more and more studies on air curtains appeared in the literature, labeling it as an effective way to confine smoke. Hiroshi et al.[9] conducted a 1/60 small scale experiment to investigate the operation of a single type air shutter in a corridor. They suggested that the air shutter flow

based on push-pull principle is an excellent aid to fire defense systems. Guyonnaud et al.[10] discussed some design information on the air curtain by conducting a bench experiment as well. Utilization of air curtain for heat confinement was also discussed by numerical simulations [11, 12].

A few publications were also found in which Fire Dynamics Simulator (FDS) was used for investigating air curtain flows with CFD [13-15], from which it can be concluded that air curtains are useful for confinement of smoke during an accidental fire. However, the following aspects are new in the present paper, compared to [13-15]:

- The latest version (6.0.1) of FDS is used; compared to the previous versions, the turbulence modeling has been updated substantially (along with, e.g., combustion modeling and radiation modeling, but this is not relevant for the study at hand);
- The main focus is on the impact of the velocity inlet boundary condition in the near-field region;
- The mesh sensitivity of the results is discussed.

2. General set-up of the simulations

In the present work, Large Eddy Simulations (LES) as implemented in the Fire Dynamics Simulator (FDS), Version 6.0.1[16], are used to perform the CFD simulations. The Deardorff turbulence model ($C_v = 0.1$) [17] is applied in the present study.

Different computational domains have been used, depending on the length (L) of the air slot. Figure 1 shows computational domain III, for L= 40cm. Table 1 provides an overview with details for the four computational domains. For the first 3 cases, the domain width (W_d) and the domain height (H_d) equal 10 cm, which is 5 times the slot width (W = 2 cm). This is sufficient to investigate on the near-field jet flow region. For the far-field region, domain IV (W_d = 40cm and H_d = 100cm) is adopted. Cubic cells are used in all simulations. The number of cells across the orifice width varies from 1 to 10, i.e., the cell size varies from 2cm to 0.2cm.

The top and four side boundaries of the domain are open to the outside by specifying it to be 'OPEN'. The floor (marked in yellow) is a 'solid' boundary condition. The orifice ('VENT'), marked in green, lies in the middle of the floor and has a velocity inlet boundary condition. The prescribed velocity value is 5m/s in all simulations, intended as a top hat velocity profile. A set of velocity detectors, set at intervals of 1cm in the vertical symmetry plane, is marked in blue.
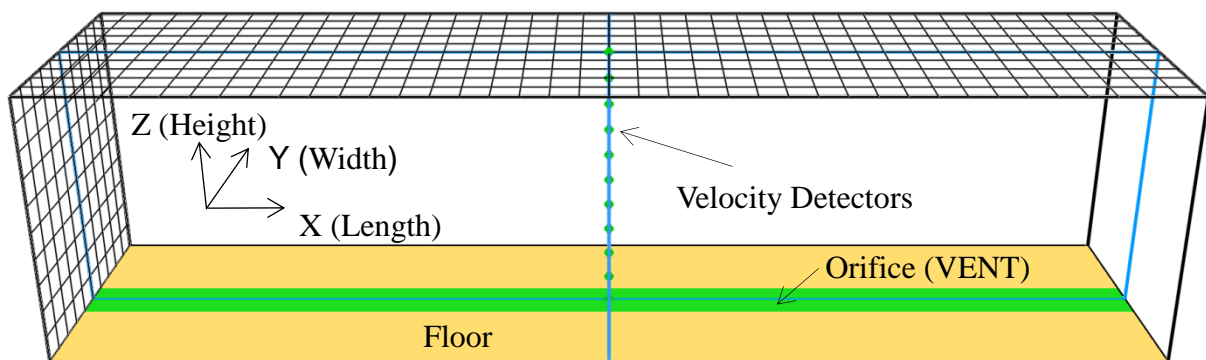

Figure 1. Sketch of computational domain III, configuration A.

Table 1. Overview of characteristics of computational domains.

Domain number	Domain length L_d (cm)	Orifice Length L (cm)	Number of cells across the orifice width
I	10	2, 4, 6, 8, 10	1, 2, 3, 4, 5, 8, 10
II	20	12, 16, 20	1, 2, 3, 4, 5, 8, 10
III	40	40	1, 2, 3, 4, 5, 8, 10
IV	50	40	5

3. Implementation and visualization of the inlet velocity boundary condition

It is instructive to carefully examine how the velocity inlet boundary condition is implemented in FDS, version 6.0.1, in a configuration as sketched in Figure 1. Obviously, the reader is referred to the FDS manuals for detailed information. Yet, a discussion is devoted to this topic, since the visualization through output does not fully reflect the implementation, due to the introduction of interpolation errors (distributing staggered velocity values to values on the corners of mesh cells). If the mesh is too coarse, this can be misleading, as illustrated below.

One single velocity value (V_{input}) is specified, so a top-hat profile can be expected for the mean velocity. On the other hand, no-slip conditions are enforced at walls. Consequently, the question arises how this affects the inlet velocity profile. Another aspect still is how this is visualized (through Smokeview). In order to investigate this, a separate study is performed first with a square orifice (with dimension 2cm x 2cm) in computational domain I. The imposed velocity in the input file is $V_{input} = 5$m/s.

Figure 2 displays mean velocity contours with averaging period of the last 1 second of the calculation time in the inlet plane, retrieved as output from the simulations, for different mesh cell sizes. The results as presented have been distilled from 'slice file' data. An evolution in the velocity is clearly observed from zero to V_{input} from one cell-width outside the geometrically defined orifice to one cell-width inside the geometrically defined orifice. This has a number of consequences. First of all, the imposed velocity V_{input} can only be found in the inner region of the orifice if 3 cells or more are used across the orifice width (in fact, in Fig. 2 the value of 5 m/s is only seen in the legend from figure e onward). This is confirmed in Figure 4 below, showing the ratio of the mean velocity as retrieved as output in the center of the orifice (V_{output}) to V_{input}. At least 5 cells across the orifice width are required to reduce the deviation below 3% for the case L / W = 1. However, as mentioned before, the deviations observed are primarily due to 'interpolation' errors, i.e. the velocities, stored in a staggered manner in FDS, are 5m/s in each cell in the inlet.

Secondly, the velocity gradient observed in Fig. 2, can also be interpreted as a change in 'effective' cross-sectional area of the orifice. Indeed, assuming that the solid boundary limit is at the position where the velocity equals zero, the effective area is always larger than the geometrically defined area. Moreover, the effective area depends on the mesh cell size. The deviation between the effective area and the geometrically defined area becomes smaller as the mesh becomes finer. Yet, as soon as the effective area differs from the geometrically defined area, it becomes impossible to keep both the mass flow rate and the momentum flow rate unchanged. This is discussed in more detail in the next subsection.
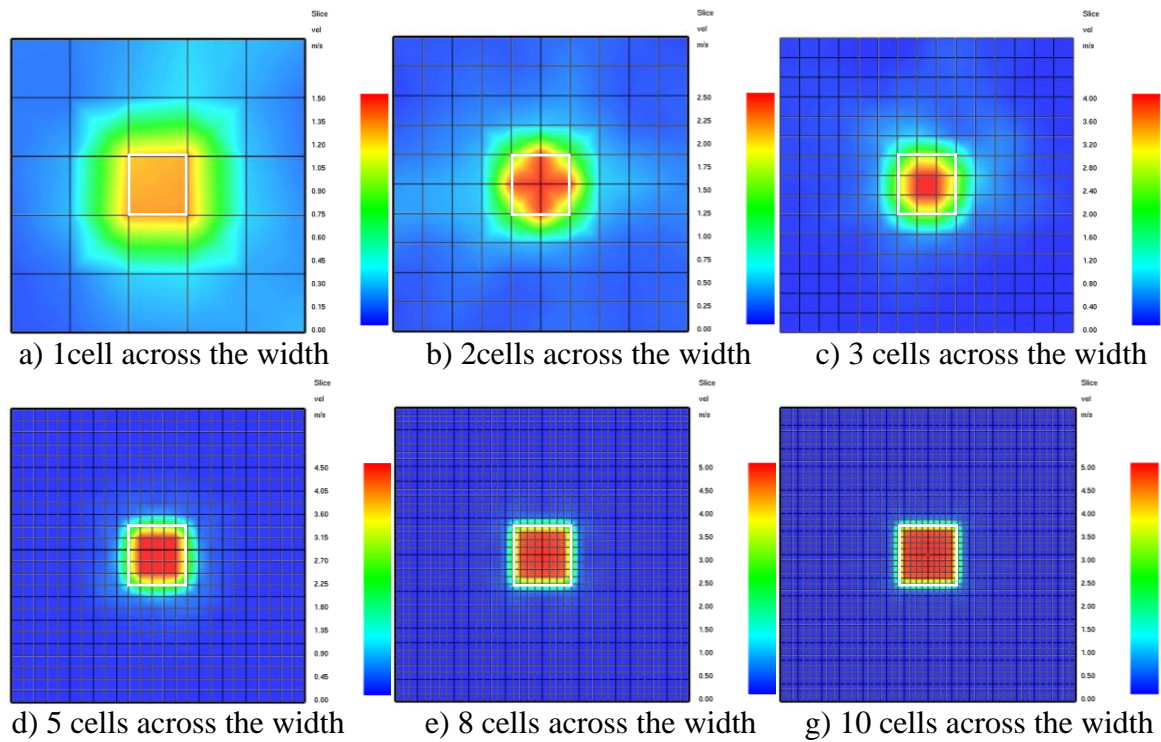
a) 1cell across the width b) 2cells across the width c) 3 cells across the width

d) 5 cells across the width e) 8 cells across the width g) 10 cells across the width

Figure 2. Contours of mean velocity, retrieved as output in the inlet plane, in computational mesh I, configuration A. The square orifice has a width W = 2cm. The velocity, implemented in a staggered manner in FDS, is constant across the inlet (5m/s).

Figure 3 presents the results as 2D profiles. The evolution towards a top-hat profile is clearly observed as the mesh becomes finer. At the same time, very strong deviations are observed if only 1 cell is used across the orifice width.
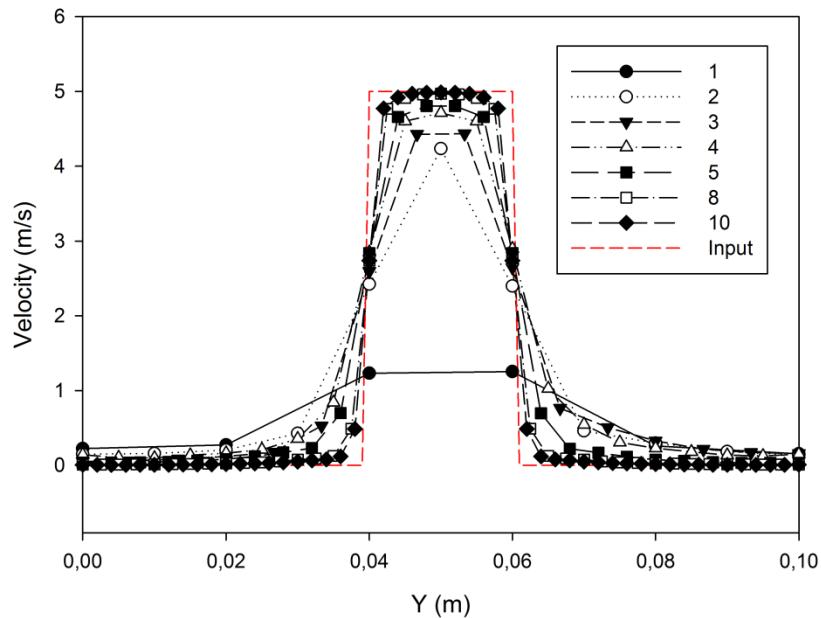
Figure 3. Impact of mesh size on the inlet velocity profile, retrieved as output in the inlet plane, in computational mesh I, configuration A. The square orifice has a width W = 2cm. The velocity, implemented in a staggered manner in FDS, is constant across the inlet (5m/s).

As mentioned, Figure 4 shows the sensitivity on the mesh of the ratio of the mean velocity in the center of the orifice as actually retrieved from the output (V_{output}) to the value imposed in the input file (V_{input}), for configurations as sketched in Figure 1. Square cells are used in all configurations, so that more cells are effectively applied within the orifice as L/W increases. This explains the increase in V_{output}/ V_{input} as L/W increases. Figure 4 illustrates 'grid convergence': the ratio V_{output}/ V_{input} approaches unity as the mesh becomes finer, as it should be. At least 5 cells are required across W to guarantee deviations (read: interpolation errors) of less than 3%.
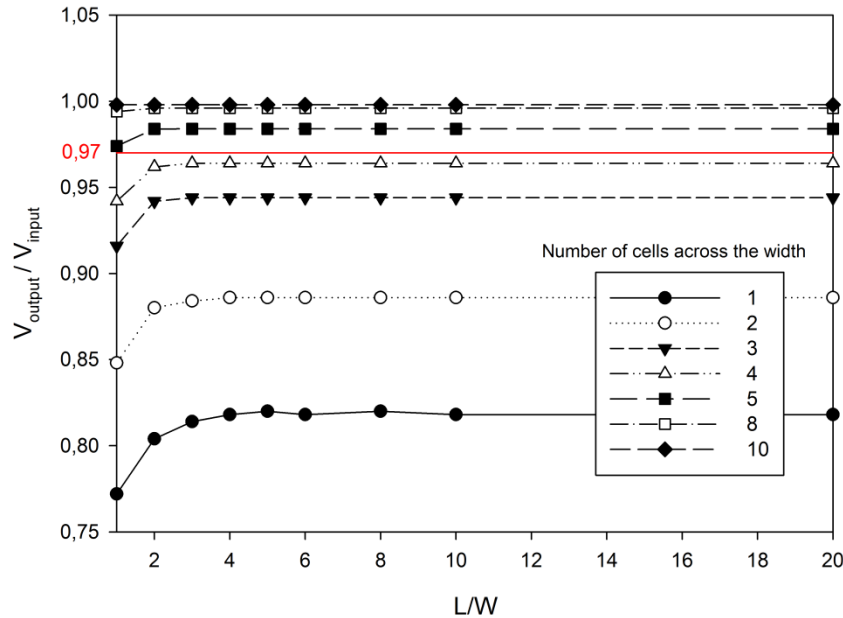

Figure 4. Impact of the mesh on the ratio V_{output}/ V_{input} for different orifice dimensions.

A consequence of the fact that the 'effective' orifice area in the output seemingly does not match the geometrically defined area, is that the mass flow rate and momentum flow rate might not seem 'correct' (i.e., in agreement with what is envisaged in the input file). This is discussed in Figure 5. The dashed line refers to the values with top hat profiles, using V_{input}. This line corresponds to what is truly implemented in FDS as well, storing velocities in a staggered manner. In other words: the 'correct' mass and momentum flow rates are imposed at the inlet. The 'output' results for mass flow rate and momentum flow rate have been obtained by integrating piecewise linearly interpolated velocity profiles, using the mean values as retrieved from the output file.

Figure 5 reveals that the correct mass flow rate is retrieved from the output files. In other words, as expected, the linear interpolation of the staggered velocities to the mesh cell corners, does not affect the integration of the volume (or mass) flow rate.

However, apparent deviations for the momentum flow rate are observed. Indeed, the fact that the velocity profile has a smooth gradient (which depends on the mesh size, as mentioned above, see Figure 3), rather than a top-hat profile, is felt in the momentum flow rate, as the velocities are squared in the integrand. Over-all, less momentum flow rate seems to be injected into the domain than what would be obtained with a top-hat profile. Figure 5 does reveal grid convergence. Yet, in practical CFD simulations, the number of cells across the orifice width will probably be 5 (or less), so the user should be aware of the implications at the level of observed momentum flow rate in the output file.

To conclude this discussion, it is mentioned that, regardless the mesh size, the correct mass and momentum flow rates are injected into the domain in the FDS simulations, but the

output as retrieved from slice files can be misleading, particularly for coarse meshes, due to interpolation errors.
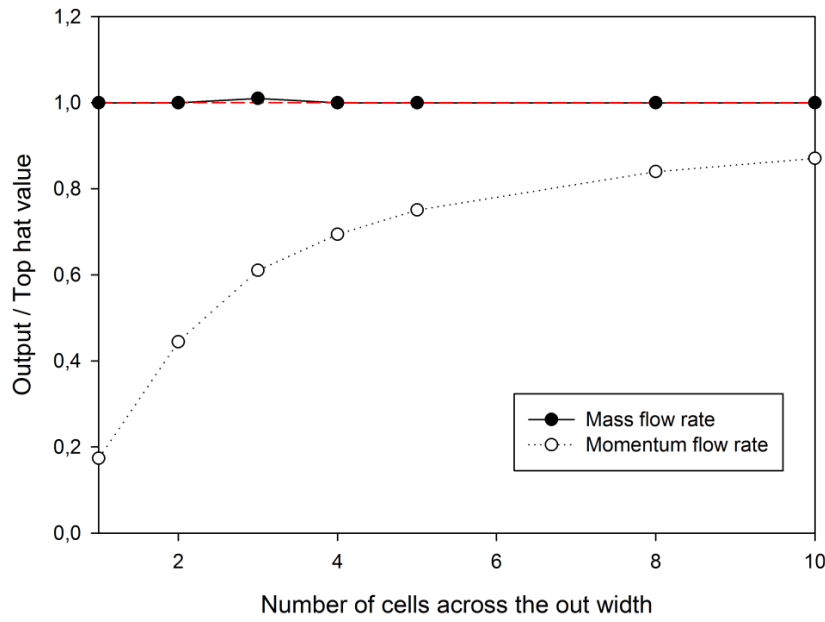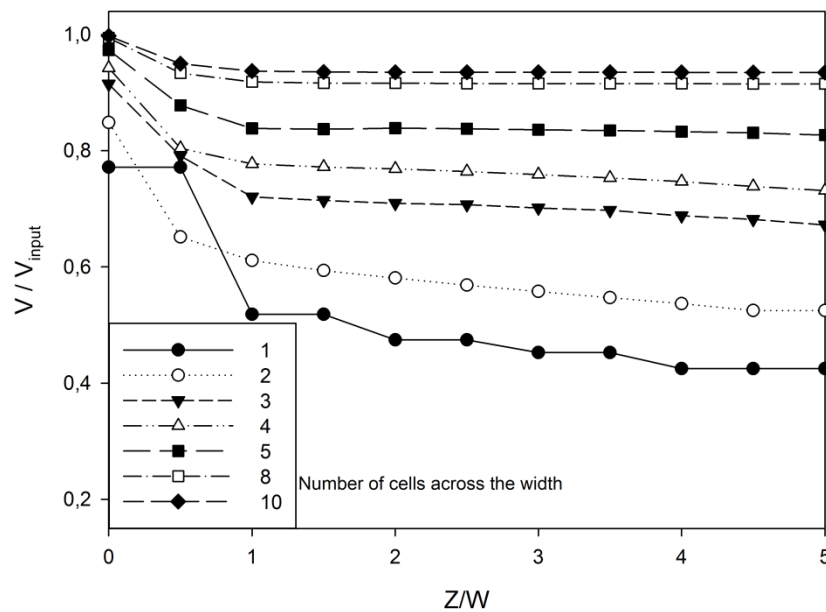

Figure 5. Impact of the number of cells across the orifice width on the ratio of mass flow rate and momentum flow rate, retrieved as output, to the corresponding values for top-hat profiles with V_{input} for configuration A (L/W = 1).

4. Orifice Configurations
4.1 Near field region
Figure 6 presents the evolution of the mean velocity on the centerline in the computational domain in the potential core region. The impact of the mesh size is visible. The variation in inlet velocity (at Z = 0), as obtained from the output, has been explained above. However, the bottom figure of Fig. 6 rules out the differences at the inlet (by normalizing the velocity, using the output value at the inlet). It suggests higher momentum flow rates as the mesh gets finer (in agreement with Fig. 5): the velocity decays less rapidly as the mesh gets finer. Figure 6 reveals a drop in velocity near the orifice in all curves. This is discussed next.
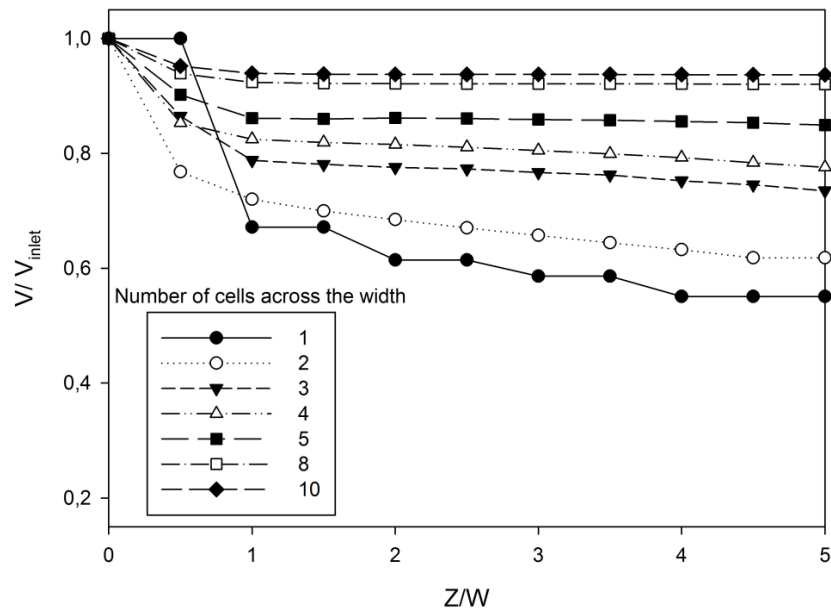
Figure 6. Impact of the number of cells across the orifice width on the evolution of the centerline velocity with distance from orifice for configuration A (L/W = 1). Top: output velocity, divided by imposed inlet velocity; bottom: output velocity, divided by output velocity at the inlet.

So far, the discussion has been restricted to the situation where the orifice is flush with the floor and the inlet velocity boundary condition is imposed in that plane ('configuration A', Figure 1). Figure 7 illustrates 2 other configurations. In 'configuration B', a duct is added, so that the velocity inlet boundary condition is imposed upstream of the actual orifice. In this case, there is an evolution from the top-hat profile at the inlet of the domain to a profile that emerges from the orifice. Obviously, the length of the duct will affect the velocity profile, as long as the flow is not fully developed inside the duct. This is discussed below. 'Configuration C' (Figure 7, right) has been added to this study in order to examine the vena contracta effect at the orifice exit.
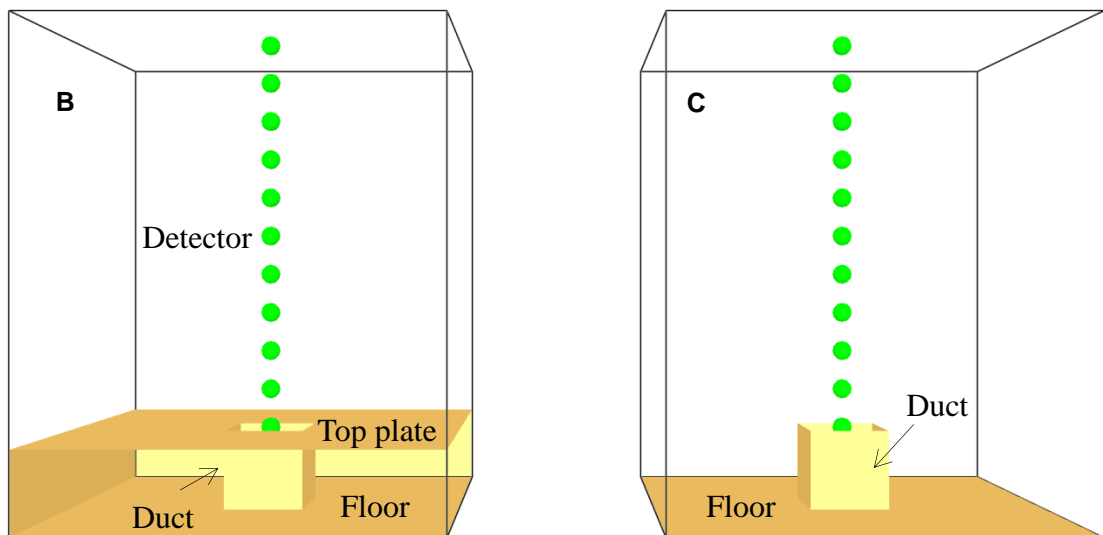

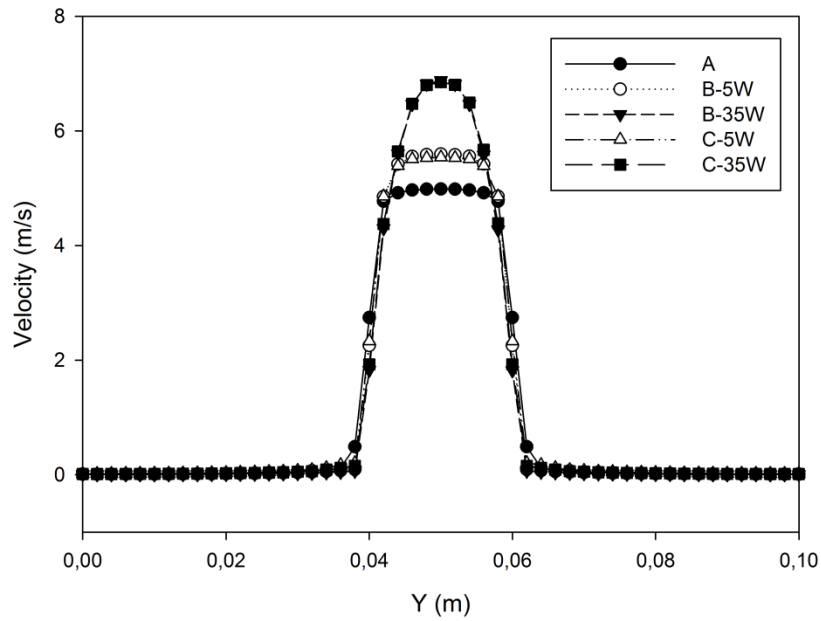**Figure 7**. Sketch of configuration B (left) and C (right).

Figure 8. Impact of configuration and duct length on the inlet velocity profile, retrieved as output in the inlet plane. The square orifice has a width W = 2cm.

Figure 8 illustrates the impact of the duct length and the configuration on the velocity profile, emerging from the orifice. Ten cells have been applied across the orifice width. For configurations B and C, many different duct lengths have been simulated. A duct length of approximately 15 hydraulic diameters is required to obtain a fully developed flow inside the duct, starting from the imposed single velocity value (not shown here). Fig. 8 shows results for only 2 duct lengths, namely 5W and 35W. In the latter, the flow is fully developed, whereas in the former the flow is still accelerating in the middle of the duct as it emerges from the orifice.
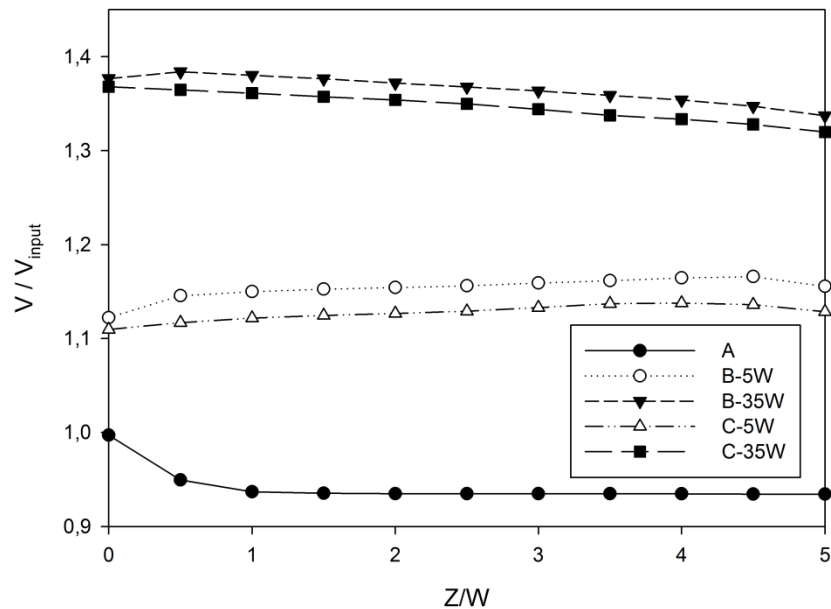

Figure 9. Impact of the orifice configuration on the evolution of the centerline velocity with distance from orifice (L/W = 1). The labels '5W' and '35W' in the legend refer to the length of the duct (Figure 7).

Figure 9 reveals the impact of the configuration on the evolution of the centerline velocity with distance from orifice. The following can be concluded:

- The drop in centerline velocity is only observed in configuration A. This is a caveat when CFD simulations are performed.

- With configuration B, a sudden increase is observed near the orifice. For the case where the duct length is only 5W, this increase is the combined effect of the accelerating flow inside the duct and a (small) vena contracta effect as the flow emerges from the duct. Indeed, the increase in velocity is less pronounced when the duct length equals 35W (and the flow is no longer accelerating inside the duct).

- In configuration C, there is no vena contracta effect, as the co-flow is well aligned with the flow emerging from the nozzle. Consequently, no increase in velocity is observed if the duct length is long enough for the flow to be fully developed inside the duct (see curve 'C – 35W'). The observed increase for curve 'C – 5W' is due to the fact that the flow is still accelerating inside the duct.

4.2 Far-field region

In this section, it is briefly illustrated that the self-similarity in the far-field region is captured well in the FDS 6.0.1 simulations, regardless the nozzle configuration. As mentioned in section 2, computational domain IV has been used. Normalized mean velocity profiles at a few selected downstream locations Z/W are presented in Fig.10. The jet half-width is noted as $y_{0.5m}$. The Gaussian distribution $U_n = e^{-\ln 2 (y_n)^2}$ has been added for comparison reasons [18, 19].
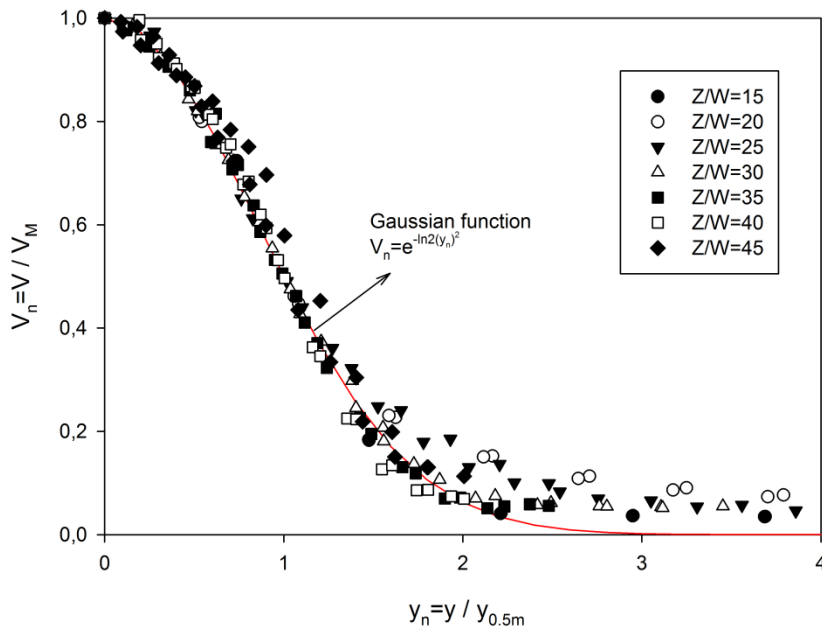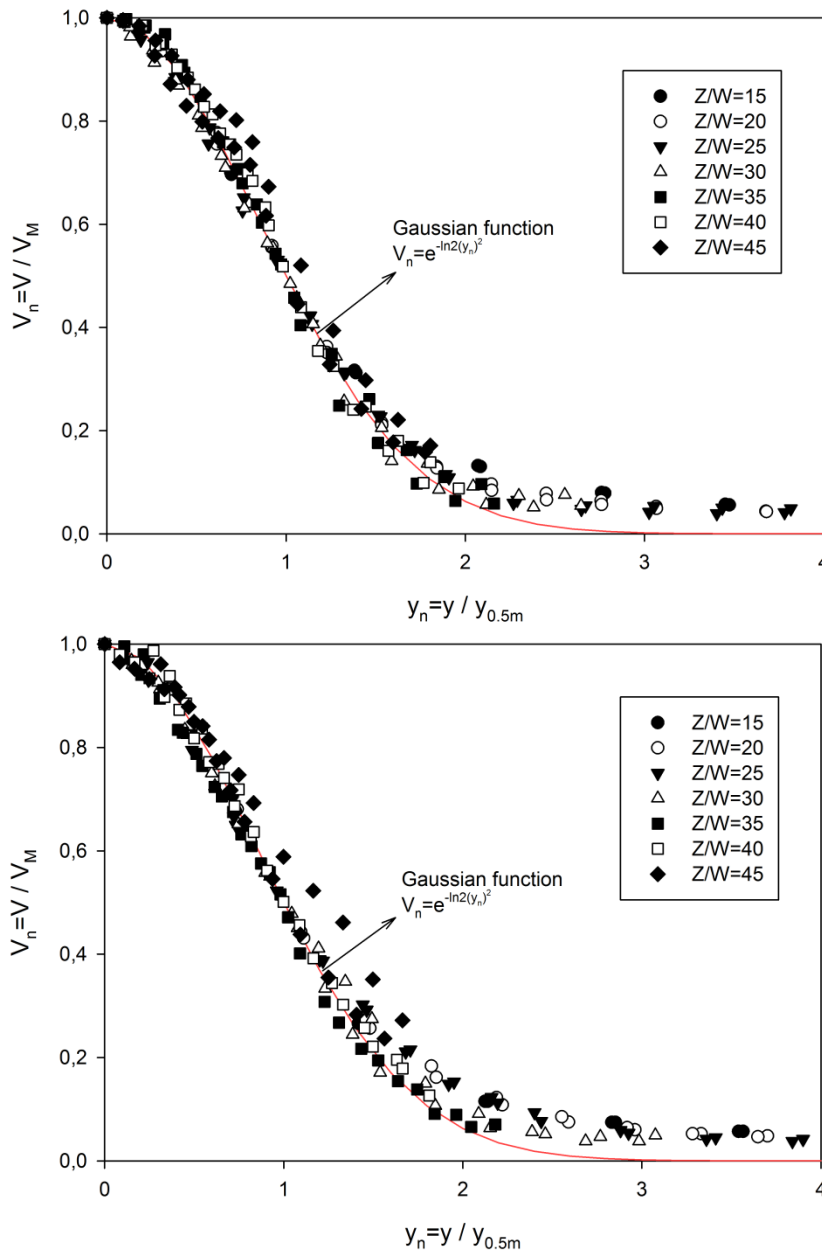
Figure 10. Normalized profiles in the self-similar region for configuration A (top), B (middle) and C (bottom).

5. Conclusions

An analysis has been conducted on the impact of the velocity inlet boundary condition, in combination with the mesh size, on the flow field in the near-field region, using FDS, Version 6.0.1. The following can be concluded:

- Although the correct mass and momentum flow rates are injected in the FDS simulations through a staggered approach, interpolation errors can result in misleading observations in the output. Velocity gradients suggest an under-prediction in momentum flow rate in the output. Grid convergence is observed, though. The potentially misleading observations can be avoided through the use of the recently defined quantities, including the word 'WALL', specifically defined for use at solid boundaries, in FDS6.* versions [17] (e.g. 'MASS FLOW WALL' for the mass flow rate).
- Providing a duct ahead of the orifice exit in the simulations, a small vena contracta

effect is observed when the orifice is flush with a solid boundary. This vena contracta effect correctly disappears if the co-flow is aligned with the jet flow at the orifice exit.

- A duct length of about 15 hydraulic diameters is required for the flow to become fully developed inside the duct, starting from a top hat velocity profile at the inlet.

- A drop in the centerline velocity evolution is observed if the inlet velocity boundary condition is imposed in the orifice exit. Thus, attention should be paid to the precise implementation of the inlet boundary conditions when CFD simulations are performed.

- Self-similarity in the far-field region is captured well in the FDS simulations, regardless of the inlet configuration.

Acknowledgements

References

[1] Moriyama S, Smoke Control System for High-Rise Buildings in Japan, Journal of Disaster Research, 2011;6: 551-52.

[2] Sato K, Gas screening effect caused by steam curtains, Journal of Loss Prevention in the Process Industries, 1989;2: 209-14.

[3] Oliveira L, Costa J, Carvalho M, Gerhardt H, Kramer C, On aerodynamic sealing for industrial applications, Journal of Wind Engineering and Industrial Aerodynamics, 1991;37: 255-68.

[4] Ciocănea A, Dragomirescu A, Modular ventilation with twin air curtains for reducing dispersed pollution, Tunnelling and Underground Space Technology, 2013;37: 180-98.

[5] Shih Y-C, Yang A-S, Lu C-W, Using air curtain to control pollutant spreading for emergency management in a cleanroom, Building and Environment, 2011;46: 1104-14.

[6] Foster AM, Barrett R, James SJ, Swain MJ, Measurement and prediction of air movement through doorways in refrigerated rooms, International Journal of Refrigeration, 2002;25: 1102-09.

[7] Foster AM, Madge M, Evans JA, The use of CFD to improve the performance of a chilled multi-deck retail display cabinet, International Journal of Refrigeration, 2005;28: 698-705.

[8] Standard PsRoCMI. Air curtain. In. Air curtain. Beijing, China Standard Press, 1999, pp. 3-4.

[9] Sakurai H, Hayashi T, Shibata M, Kanehara K, Researches on air shutter for fire defence, Fire Safety Journal, 1980;2: 9-16.

[10] Guyonnaud L, Solliec C, de Virel MD, Rey C, Design of air curtains used for area confinement in tunnels, Experiments in Fluids, 2000;28: 377-84.

[11] Elicer-Cortés JC, Demarco R, Valencia A, Pavageau M, Heat confinement in tunnels between two double-stream twin-jet air curtains, International Communications in Heat and Mass Transfer, 2009;36: 438-44.

[12] Felis F, Pavageau M, Elicer-Cortés JC, Dassonville T, Simultaneous measurements of temperature and velocity fluctuations in a double stream-twin jet air curtain for heat confinement in case of tunnel fire, International Communications in Heat and Mass Transfer, 2010;37: 1191-96.

[13] Hu LH, Fong NK, Yang LZ, Chow WK, Li YZ, Huo R, Modeling fire-induced smoke

spread and carbon monoxide transportation in a long channel: Fire Dynamics Simulator comparisons with measured data, Journal of Hazardous Materials, 2007;140: 293-98.

[14] Hu LH, Zhou JW, Huo R, Peng W, Wang HB, Confinement of fire-induced smoke and carbon monoxide transportation by air curtain in channels, Journal of Hazardous Materials, 2008;156: 327-34.

[15] Luo N, Li A, Gao R, Zhang W, Tian Z, An experiment and simulation of smoke confinement utilizing an air curtain, Safety Science, 2013;59: 10-18.

[16] McGrattan K, Hostikka S, Floyd J, Mell W, McDermott R, Fire dynamics simulator, technical reference guide, volume 1: mathematical model, NIST special publication, 2013;1018.

[17] McGrattan KB, Hostikka S, Floyd J, Fire Dynamics Simulator, User's Guide, NIST special publication, 2013;1019.

[18] Pope SB, Turbulent flows, Cambridge university press, 2000.

[19] Deo RC, Mi J, Nathan GJ, The influence of nozzle-exit geometric profile on statistical properties of a turbulent plane jet, Experimental Thermal and Fluid Science, 2007;32: 545-59.